Materials Science-Poland, 40(3), 2022, pp. 112-124
http://www.materialsscience.pwr.wroc.pl/
DOI: 10.2478/msp-2022-0036

Fabrication, microstructure, and machinability of aluminum metal-matrix composites

S. Kathiravan[1], R. Thanigaivelan[2,*], P. Suresh[3]

[1]Department of Mechanical Engineering, Alpha College of Engineering, Chennai-600124, India
[2]Department of Mechanical Engineering, AKT Memorial College of Engineering and Technology, Kallakurichi-606213, India
[3]Department of Mechanical Engineering, Muthayammal Engineering College (Autonomous), Rasipuram-637408, India

Today, researchers across the world focus on sustainable products, and, accordingly, it is now imperative to develop sustainable MMCs. In line with this, ongoing experimental work aims to fabricate aluminum 6061 MMC with ground granulated blast furnace slag (GGBS) and study the micro-structural and machinability characteristics. A liquid state stir casting setup is used to melt aluminum 6061 alloy and reinforced with 2.5 wt.%, 5.0 wt.%, and 7.5 wt.% of GGBS. X-ray diffraction (XRD) studies were used to identify the chemical elements that were present in the fabricated samples. In order to observe the formation of any secondary elements, energy-dispersive X-ray spectroscopy and scanning electron microscopy (SEM) were utilized on the cast composites. Through the milling process, the influence of the GGBS reinforcement composition on the surface roughness (SR) and material removal rate (MRR) of aluminum 6061 MMC was examined, considering the parameters of spindle speed, feed rate, depth of cut, and reinforcement composition percentage. The L_9 orthogonal array (OA) was used to investigate the results of the experiments, and the Taguchi technique was used to optimize the process. The best MRR value was produced by the feed rate (B3) of 260 mm^3/min and the depth of cut (C3) of 0.75 mm. The study ascertained that the lower SR value is attained corresponding to a spindle speed of 1,250 rpm, a feed rate of 220 mm^3/min, a depth of cut of 0.25 mm, and a reinforcement composition percentage of Al 6061 with 5% GGBS.

Keywords: *aluminum, stir casting, metal-matrix composites, Taguchi, optimization*

1. Introduction

Aluminum metal-matrix composites (AMC) are gradually replacing traditional aluminum alloys in numerous applications due to their high strength-to-weight ratio, wear resistance, good corrosion, low thermal expansion, and other benefits [1]. Ex-situ and in-situ methods are used to incorporate ceramic particles such as B_4C, TiB_2, ZrB_2, SiC, Al_2O_3, and others into the aluminum matrix. AMC processing plays a critical role in achieving good mechanical properties. Depending on the type, size, and morphology of the reinforcement, the AMCs are manufactured using liquid state processing methods such as stir casting, squeeze casting, spray deposition, and compo casting, as well as solid state processing methods such as powder metallurgy and mechanical alloying [2]. Liquid state processing is one of the most effective methods due to its ease of implementation, simplicity, and productivity [3]. Due to the low density of reinforcement particles in the matrix, most ex-situ AMCs have low matrix-reinforcement bonding strength. Exothermic reactions of specific metallic powders or inorganic salts with molten melt at a specific temperature result in in-situ particles. The in-situ method makes sure that particles are evenly distributed throughout the matrix and that the reinforcement and matrix have stronger interfacial bonds. The high thermodynamic stability of in-situ formed particles also helps to reduce undesirable phases in in-situ composites. In order to achieve all of these advantages, the in-situ fabrication method is utilized in this study [4]. Dinaharan et al. [5] employed the in-situ fabrication method in relation to the processing of AA6061/ZrB_2 composites, and their results demonstrated that hardness, wear resistance, and ultimate tensile strength were significantly improved. When K_2ZrF_6 and KBF_4 salts re-

* E-mail: tvelan10@gmail.com

© S. Kathiravan et al. 2022. This is an open access article distributed under the Creative Commons Attribution-NonCommercial-NoDerivatives 4.0 License. (http://creativecommons.org/licenses/by-nc-nd/4.0/)

acted in-situ to form ZrB_2 particles, Naveen Kumar et al. [6] fabricated AA6351 metal-matrix composites (MMCs) reinforced with these particles and noticed that as the volume fraction of ZrB_2 particles increased, the AMCs' hardness and wear resistance. Michael Rajan et al. [7] formed in-situ AA7075/TiB_2 composites, and they reported that the TiB_2 particles were evenly dispersed throughout the composite and dramatically improved mechanical properties while raising TiB_2 particle content. TiB_2/7055 in-situ composites were made by Zhong et al. [8], who discovered that the uniform distribution of spherical or hexagonal-shaped TiB_2 particles throughout the matrix decreased the (Al) phase's grain size. Zhang et al. [9] used a magneto-chemical in-situ molten reaction to make (Al_3Zr + ZrB_2)/Al composites and found that increasing the percentage of reinforcements reduced wear weight loss. Al-4Cu matrix composites reinforced with Al_3Zr, ZrB_2, and Al_2O_3 particulates synthesized by magneto-chemical melt reaction were found to have significantly improved mechanical characteristics and wear resistance, according to Zhao et al. [10]. AMCs appeared to have better ductility than many other composites, according to Kumar et al. [11], who created AA5052/ZrB_2 in-situ composites.

On the other hand, MMC had improved core mechanical characteristics like toughness, harness, wear resistance, and thermal stability. The improvement of surface roughness (SR) during machining is a significant challenge. Numerous studies on the machining of MMC built from aluminum alloys have been done by different researchers. Turning, grinding, and milling are a few examples of machining types. Up to 20% silicon carbide was added by Seeman et al. [12], who also assessed the composite's machinability. However, there aren't many studies in the literature that address the optimization of milling parameters for machining MMCs made of aluminum alloys. The majority of reports archived show that machining aluminum alloy-based composites provides lower SR integrity. After milling, Reddy et al. [13] compared the surface integrity of reinforced and non-reinforced aluminum alloys. Compared to other polymer MMC (PMMCs), aluminum alloy-based PMMCs guarantee better machining. A four-stage method was developed by Kuram and Ozcelik [14] to investigate parameter optimization during milling. Experimental modeling is one of the techniques, followed by single- and multi-objective optimization. The Taguchi technique is used by the majority of researchers to obtain optimized cutting parameters. It improves both efficient machining operations and the quality of the machined surface.

It is evident from the literature that development, mechanical property, and machinability studies on AMCs are sparse, and moreover that the use of ground granulated blast furnace slag (GGBS) material, which is a power plant waste, as reinforcement allows fulfillment of the attributes of waste recycling and low product cost. Thus, in this study, AMCs were fabricated with 2.5 wt.%, 5.0 wt.%, and 7.5 wt.% of GGBS reinforcement. Using the milling process, the influence of the GGBS reinforcement composition on the SR and material removal rate (MRR) of AMC was examined. The milling parameters, namely spindle speed, feed rate, depth of cut, and reinforcement composition percentage, were considered. The L_9 orthogonal array (OA) was used to investigate the results of the experiments, and the Taguchi technique was used to optimize the process.

2. Experimentation

2.1. Fabrication of composite

By using an in-situ fabrication technique, Al 6061 rods with a diameter of 25 mm were used as a matrix and GGBS particles as reinforcement. Table 1 shows the chemical composition of a sample matrix. The Al 6061 rods were measured and melted in an electric furnace in a graphite crucible. To avoid contamination, the inside of the chosen crucible was coated with WOLFRAKOT. The melt temperature was maintained at 900°C for Al 6061 and preheating of the reinforcement of GGBS by 650°C was carried out. GGBS was added into the crucible, and the GGBS particles' size was $\backsim$ 20 μm; the chemical composition of the reinforcement added to the mix is indicated in Table 2. Every 5 min, the melt was thoroughly stirred.

Table 1. Al6061 chemical composition in percentage

Mg	Si	Fe	Cu	Cr	Zn	Mn	Ti	Al
1.20	0.80	0.70	0.40	0.35	0.25	0.15	0.15	96

Table 2. GGBS chemical composition in percentage

SiO_2	CaO	Al_2O_3	Mg O	SO_3	K_2O	Fe_2O_3	Na_2O
34.4	33.2	21.5	9.5	0.47	0.39	0.2	0.34

GGBS, ground granulated blast furnace slag

Table 3. The milling process's parameters and their levels

Symbol	Factors	Level 1	Level 2	Level 3
A	Spindle speed (rpm)	1,000	1,250	1,500
B	Feed rate (mm/min)	220	240	260
C	Depth of cut (mm)	0.25	0.50	0.75
D	Percentage of composition	2.5	5.0	7.5

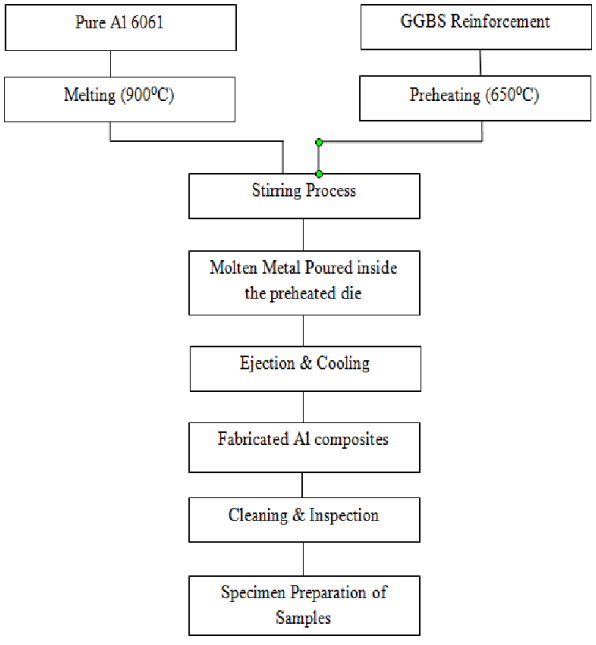


Fig. 1. Representation of Al composite fabrication. GGBS, ground granulated blast furnace slag

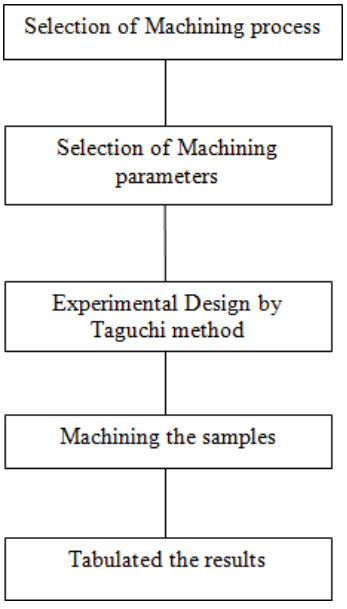


Fig. 2. Steps in machining process

Castings with a 30 min and 60 min melt holding time were carried out for the formation of different volume fractions of GGBS 2.5 wt.%, 5 wt.%, and 7.5 wt.%. Argon gas was passed through the melt to prevent oxidation, which resulted in less slag formation [15]. The slag was removed after the synthesis period was finished, and the melt was then poured into the preheated die. The cast was taken out of the die after it had fully solidified. Schematic representations of the fabrication and machining processes are illustrated in Figures 1 and 2. Figure 3 depicts the aluminum 6061 matrix material, GGBS reinforcement powder, and casted samples.

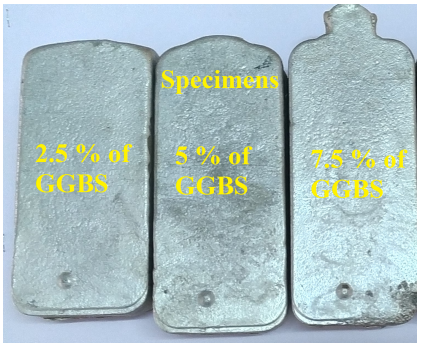
Table 4. Design of experiment using L_9 OA

Experimental No.	A	B	C	D	MRR (mm^3/min)	SR (μm)
1	1000	220	0.25	2.5	880	0.344
2	1000	240	0.50	5.0	1,920	0.340
3	1000	260	0.75	7.5	3,120	0.328
4	1250	220	0.50	7.5	1,760	0.343
5	1250	240	0.75	2.5	2,880	0.332
6	1250	260	0.25	5.0	1,040	0.356
7	1500	220	0.75	5.0	2,640	0.347
8	1500	240	0.25	7.5	960	0.347
9	1500	260	0.50	2.5	2,080	0.314

MRR, material removal rate; OA, orthogonal array; SR, surface roughness



(A)



(B)

Fig. 3. **(A)** GGBS reinforcement particles; **(B)** Different percentages of GGBS. GGBS, ground granulated blast furnace slag

2.2. Experimental design

The Taguchi techniques have been utilized to perform optimization in the current study. The experiments are planned using Taguchi's L_9 OA, the aim of deploying which is to minimize the number of experimental runs. The Taguchi method was used to evaluate performance metrics, such as MRR and SR, using input parameters such as reinforcement weight percentage, cutting speed, feed rate, and depth of cut used in milling. Table 3 lists the parameters and levels that regulate the machining process. These values were chosen based on preliminary experiments [16].

Machining performance is evaluated with MRR and SR. MRR is the rate of removal of material during machining and it is calculated based on the depth of cut, width of cut, and feed rate; here width of the cut is 16 mm. The average surface peaks and valleys across the surface are used to calculate SR. The experiments are tabulated in Table 4 and were formed by L_9 OA using Minitab 18. Higher MRR and a lower SR are preferred in the machining process.

$$\text{Material Removal Rate (MRR)} = \text{Depth of cut} * \text{Width of cut} * \text{Feed rate}$$

3. Result and discussion

3.1. Micro-structural analysis

Micro-structural investigations of samples were performed to check particle agglomeration and distribution and the formation of defects. In the various obtained samples of composites, to obtain good quality microstructures, abrasive particles are initially used for carrying out the polishing. In an aluminum matrix, particles are found to be dispersed in nature. On comparing the prepared samples, oxide particles can be identified inside Al

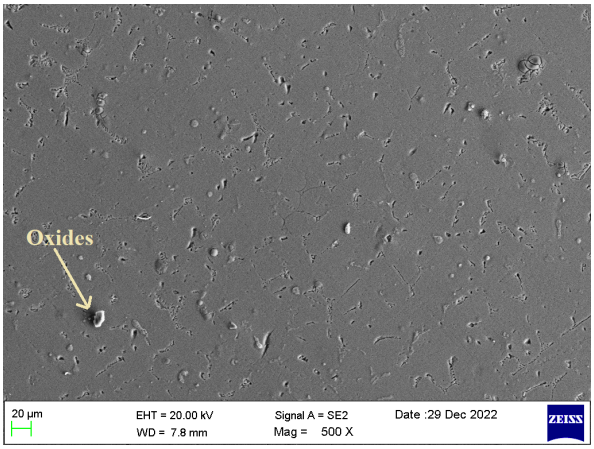


Fig. 4. SEM image of Al6061–2.5% of GGBS reinforcement. GGBS, ground granulated blast furnace slag; SEM, scanning electron microscopy

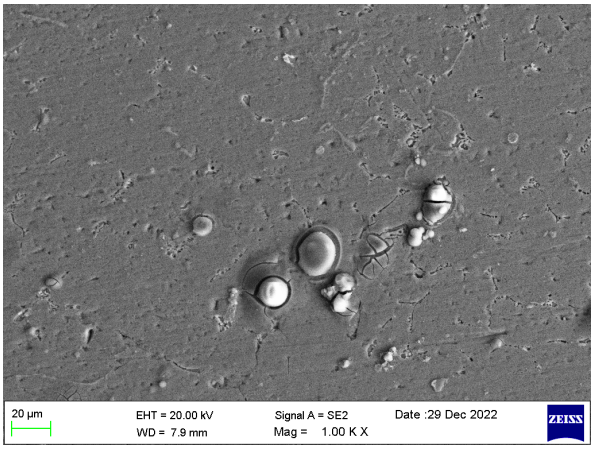


Fig. 6. SEM image of Al6061–7.5% of GGBS reinforcement. GGBS, ground granulated blast furnace slag; SEM, scanning electron microscopy

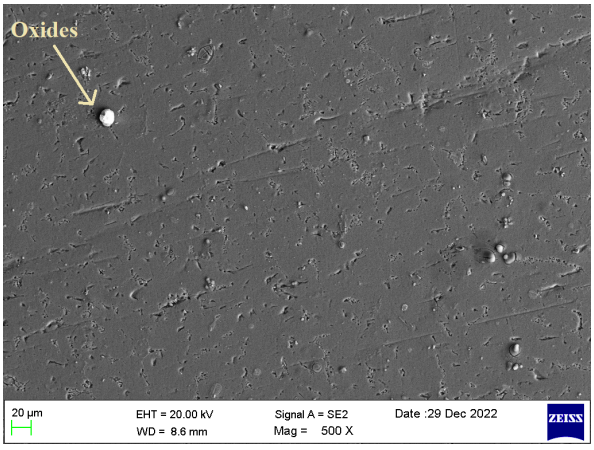


Fig. 5. SEM image of Al6061–5% of GGBS reinforcement. GGBS, ground granulated blast furnace slag; SEM, scanning electron microscopy

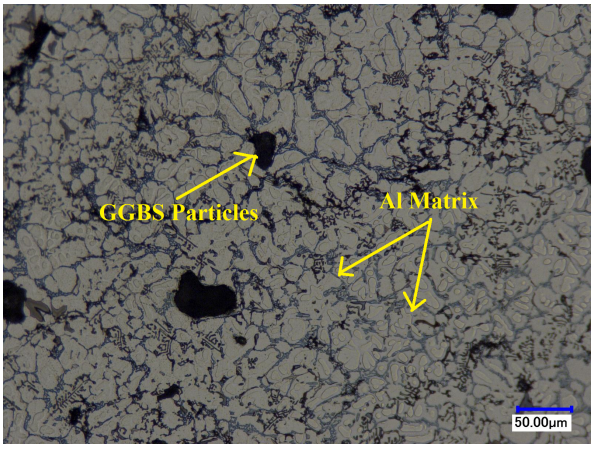


Fig. 7. Optical image of Al6061–7.5% of GGBS reinforcement. GGBS, ground granulated blast furnace slag

grains and grain boundaries. The addition of GGBS particles in samples of AMC shows clusters of silicon dioxide and oxide particles along the grain boundaries, as shown in Figure 4. Scanning electron microscopy (SEM) micrograph images confirm the presence of reinforcement particles, and also, even distribution of those particles is noticed. The separation of oxides is also noted in Figure 5. The SEM image reveals the occurrence of the distributed phase in which the calcium oxide is dispersed evenly in the matrix. There are no obvious changes in the morphology or size of the silicon dioxide and calcium particles, as observed. The grayish white-colored particles were determined to be calcium oxide, while the light gray-colored flake-like particles were determined to be Al_2O_3, as depicted in Figure 6. In addition, metallographic specimen analysis is also presented for 7.5% of GGBS reinforcement in Figure 7.

3.2. Energy-dispersive X-ray (EDX) spectroscopy

EDX spectroscopy measurements on individual specimens in the SEM are used to determine the

Table 5. Elemental results of EDX analysis

S. No.	Element	2.5% of GGBS		5.0% of GGBS		7.5% of GGBS	
		Weight (%)	Atomic (%)	Weight (%)	Atomic (%)	Weight (%)	Atomic (%)
1	O K	11.23	18.27	18.27	28.22	41.44	55.62
2	Na K	39.28	47.97	0.49	0.53	3.31	3.09
3	Al K	33.98	24.60	71.31	65.31	42.72	34.00
4	Si K	3.05	2.59	3.67	3.23	6.41	4.90
5	Cl K	6.35	4.42	0.44	0.31	0.48	0.29
6	Mn K	0.37	0.21	1.20	0.54	1.88	0.74
7	Fe K	2.00	0.71	1.05	0.47	1.82	0.70
8	Cu K	1.95	0.68	0.94	0.36	1.93	0.65

EDX, energy-dispersive X-ray; GGBS, ground granulated blast furnace slag

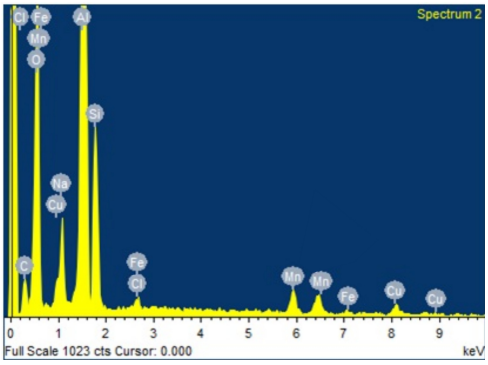


Fig. 8. SEM and EDX profile analysis for the surfaces: Al6061–2.5% of GGBS reinforcement. EDX, energy-dispersive X-ray; GGBS, ground granulated blast furnace slag; SEM, scanning electron microscopy

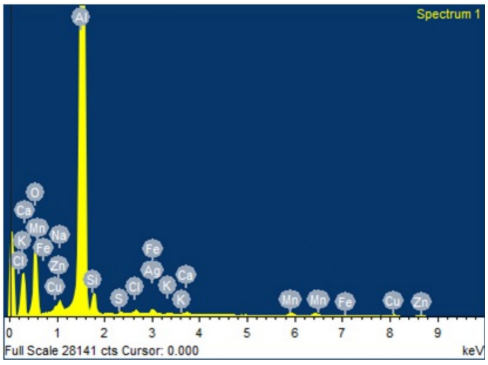


Fig. 10. SEM and EDX profile analysis for the surfaces: Al6061–7.5% of GGBS reinforcement. EDX, energy-dispersive X-ray; GGBS, ground granulated blast furnace slag; SEM; scanning electron microscopy

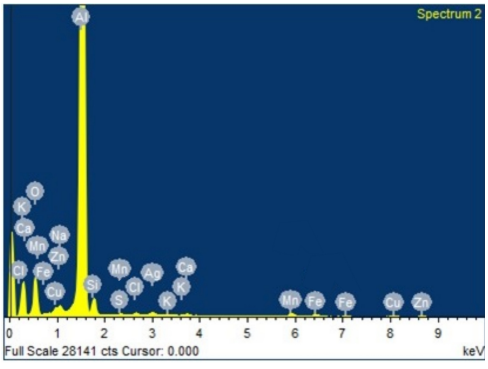


Fig. 9. SEM and EDX profile analysis for the surfaces: Al6061–5% of GGBS reinforcement. EDX, energy-dispersive X-ray; GGBS, ground granulated blast furnace slag; SEM; scanning electron microscopy

quantity of chemical composition of the Al composites. The atomic percentages of the elements found on the specimen surface are provided by the corresponding EDX profile analysis shown in Figure 8.

The presence of magnesium, copper, aluminum, silicon, zinc, and oxides in the Al6061 alloy is depicted in Figures 7 and 8. A detailed study of the interfaces in reinforced metal-matrix composites confirmed the presence of SiO_2 and Al_2O_3. Oxide content has been found in all Al6061 with GGBS reinforcement compositions. The presence of oxides is due to the formation of Al_2O_3, SiO_2, CaO, K_2O, and MgO as the major compounds in GGBS. The results of EDX examination are presented in the form of weight/atomic values for major individual elements and data concerning these are pre-

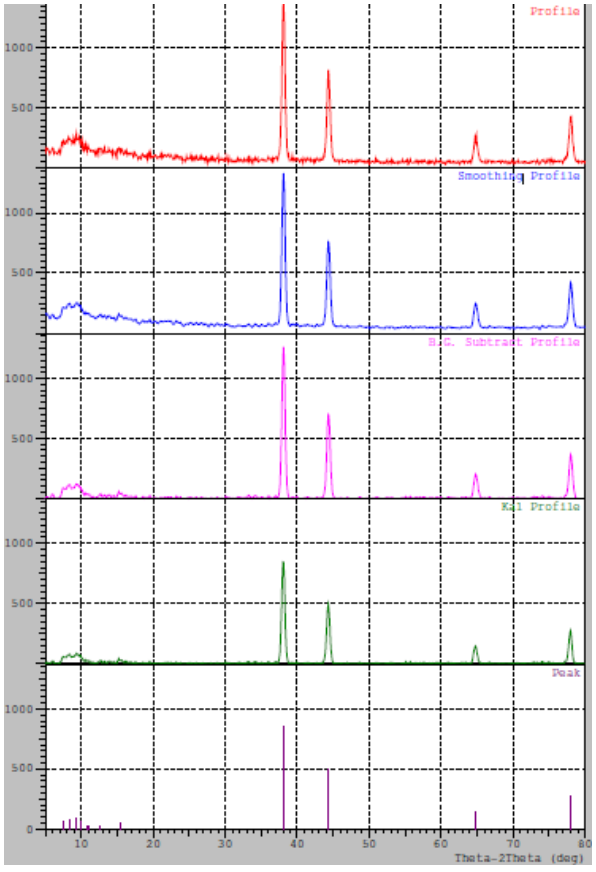


Fig. 11. XRD pattern for the surfaces: Al6061–2.5% of GGBS reinforcement. GGBS, ground granulated blast furnace slag; XRD, X-ray diffraction analysis

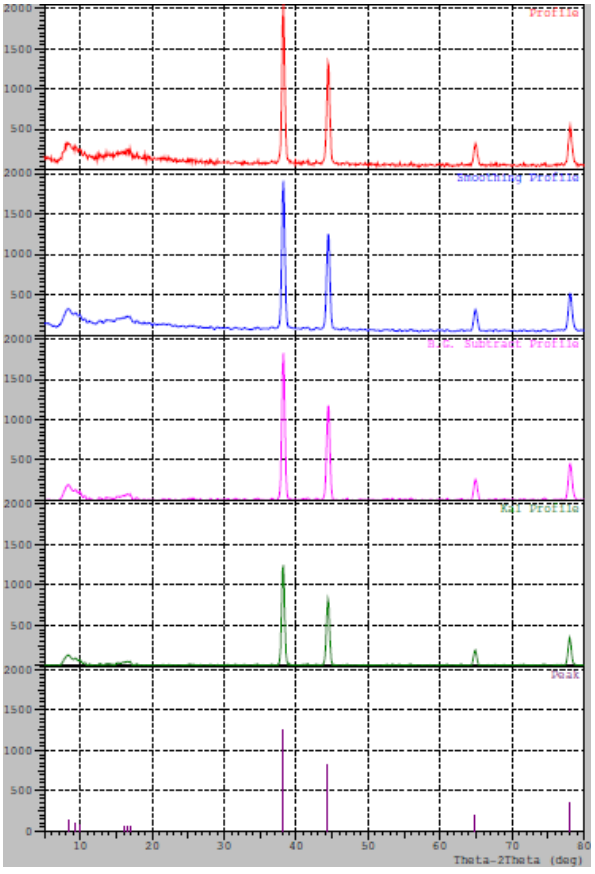


Fig. 12. XRD pattern for the surfaces: Al6061–5% of GGBS reinforcement. GGBS, ground granulated blast furnace slag; XRD, X-ray diffraction analysis

sented in Table 5. Moreover, the areas chosen for EDX analysis are also indicated in Figures 8–10. From Figures 9 and 10, it is confirmed that the percentage improvement of GGBS reinforcement increases the oxides by 18.27% for 5% of reinforcement and 41.44% for 7.5% of reinforcement. The results of EDX examination are presented in the form of weight/atomic values for major individual elements, and the corresponding data are shown in Table 5.

3.3. AMCs X-ray diffraction analysis (XRD)

Figures 11–13 depict the pattern of XRD for the fabricated samples. The peaks of the GGBS phase and the Al phase have grown, according to the XRD analysis results for the samples of Al reinforced by GGBS. In fact, the XRD analysis findings show that an increase in the weight percent of the reinforcement materials causes a rise in the diffraction peaks' intensity. According to Figures 11–13, the Al phase formed at 2θ for the planes (111), (200), and (311) in the XRD data for the pure Al (38.050, 44.310, and 77.950), respectively. Additionally, the GGBS phase was formed at 2θ (7.50°, 8.40°, and 64.75°), which denote a rise in the weight fraction of the GGBS phase and a fall in the aluminum lattice parameter.

Since there are no other compounds present, the interface between Al6061 and GGBS is easily seen. A distinct interface between the matrix and reinforcement is necessary to show that AMCs have superior mechanical properties compared to monolithic alloys [17].

Table 6. S/N ratio for MRR and SR

Levels	Parameters							
	A	B	C	D	A	B	C	D
	MRR in mm^3/min				SR in µm			
Level 1	64.81	64.08	59.63	64.81	9.441	9.252	9.144	9.636
Level 2	64.81	64.83	65.65	64.81	9.281	9.380	9.575	9.178
Level 3	64.81	65.53	69.17	64.81	9.483	9.572	9.484	9.390
Delta	0.00	1.45	9.54	0.00	0.202	0.320	0.431	0.458

MRR, material removal rate; SR, surface roughness

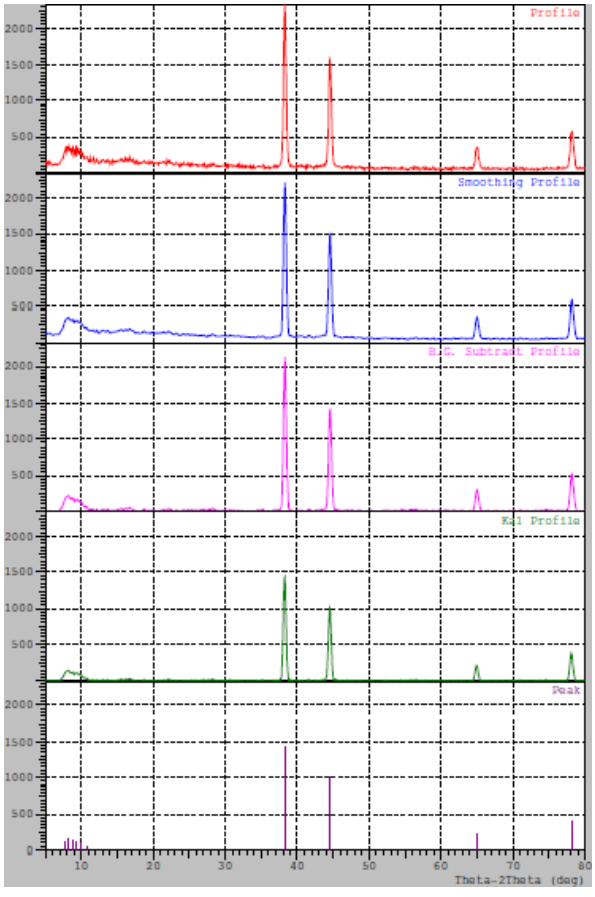


Fig. 13. XRD profile analysis for the surfaces: Al6061–7.5% of GGBS reinforcement. GGBS, ground granulated blast furnace slag; XRD, X-ray diffraction analysis

3.4. "S/N" ratio – analysis

An S/N response table is used to analyze the effects of machining factors such as reinforcement weight percentage, cutting speed, feed rate, and depth of cut on MRR and SR. Table 6 deduces the "S/N" ratio response values for MRR and SR [18].

A signal-to-noise (S/N) ratio is created by converting the values of MRR and SR [19]. The quality characteristic that deviates from the desired values is measured using this method. Based on S/N ratio analysis, for every level of the control parameter, the S/N ratio is compared. Maximizing MRR and reducing SR are the objectives of this process. Table 3 provides the values for various levels of factors for MRR and SR, and Figures 14 and 15 show the same information graphically. The best control factor and level for the MRR value are shown in the "S/N" ratios response table as S/N = 65.53 (factor B) and level 3, and S/N = 69.17 (factor C) and level 3; and other parameters like spindle speed and percentage of reinforcement composition constantly affect the MRR at all levels. The feed rate (B3) of 260 mm^3/min and the depth of cut (C3) of 0.75 mm produced the best MRR value. S/N = 9.281 (factor A) and level 2, S/N = 9.252 (factor B) and level 1, S/N = 9.144 (factor C) and level 1, and S/N = 9.178 (factor D) and level 2 were the best factors and levels for the lower SR, respectively. The best value of SR is obtained with a spindle speed (A2) of 1,250 rpm, a feed rate (B1) of 220 mm^3/min, a depth of cut (C1) of 0.25 mm, and a percent of reinforcement composition (D2) of Al 6061 T6 with 5% GGBS. Figure 15 illustrates the impact of machining parameters on the average "S/N" ratio of SR.

3.5. Experimental evaluation results

Figures 16A–16D depict the three-dimensional (3D) response surfaces for MRR and SR that change with control factors. From Figure 16A, we see depicted the effect of feed rate and depth of cut on MRR. Based on the surface plot, we are



Fig. 14. Average S/N ratio for MRR. MRR, material removal rate

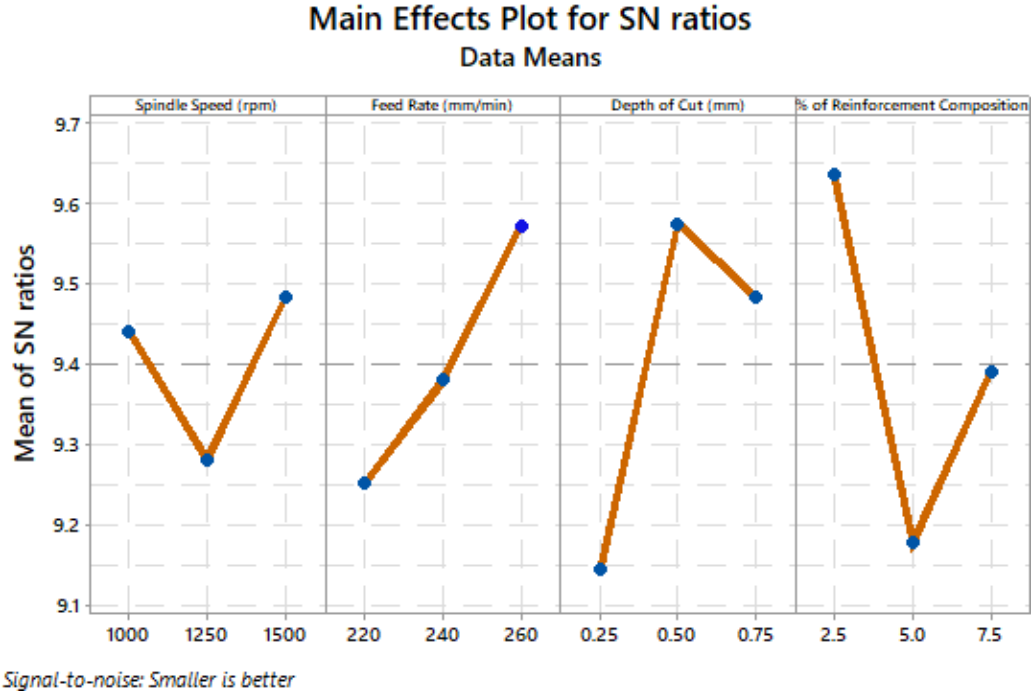
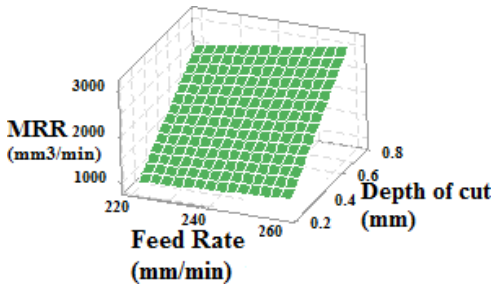
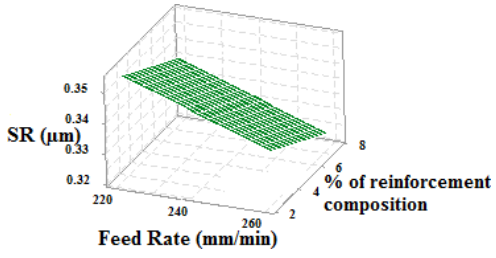


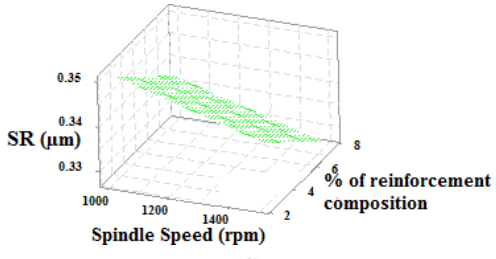
Fig. 15. Average S/N ratio for SR. SR, surface roughness



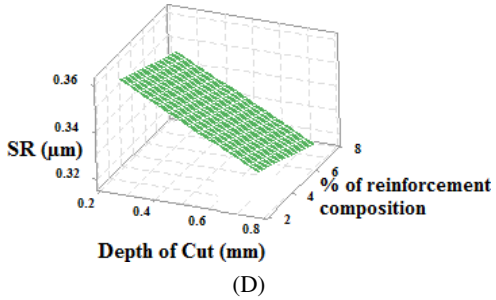
(A)



(B)



(C)



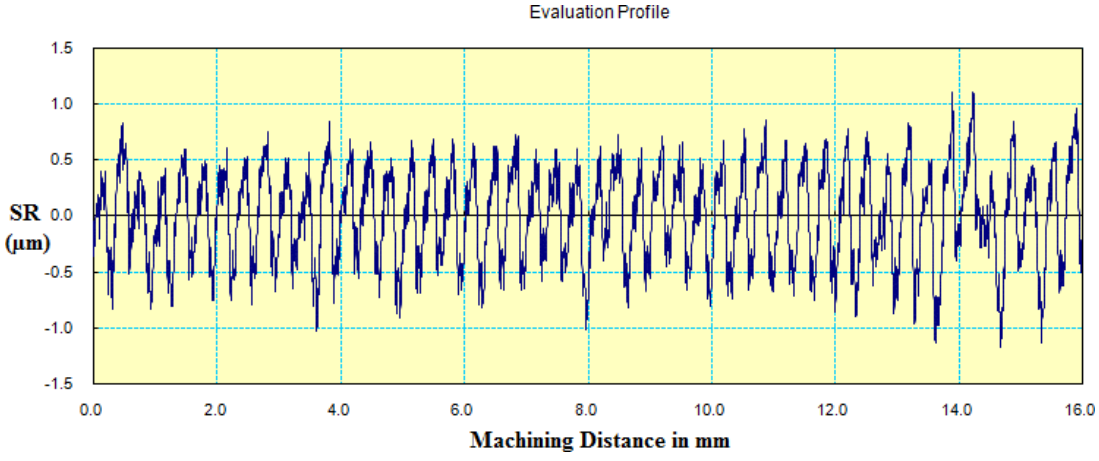
(D)

Fig. 16. Effect of parameters on **(A)** feed rate with depth of cut on MRR **(B)** feed rate with percentage of reinforcement composition on SR **(C)** percentage of reinforcement composition with spindle speed on SR **(D)** percentage of reinforcement composition with depth of cut on SR

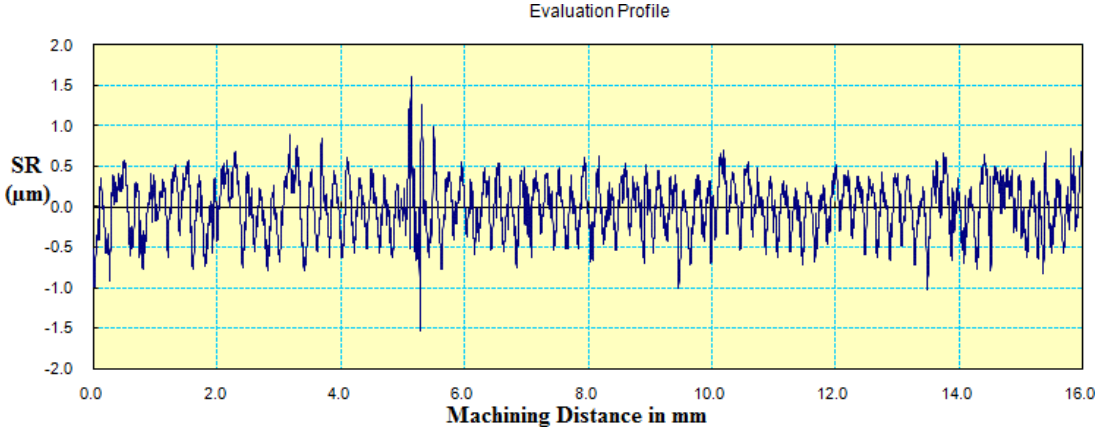
able to ascertain that as the feed rate and depth of cut increased, the MRR has also increased. The maximum feed rate of 260 mm/min and depth of cut of 0.75 mm produces the higher MRR of 3,120 mm^3/min. Hence, the other parameters like spindle speed and percentage of reinforcement composition constantly influence the MRR [20]. From Figure 16B, we see depicted the effect of feed rate and percentage of reinforcement composition on SR, which clearly illustrates that the SR will decrease when there is an increase in the percentage of reinforcement composition. Similarly, from Figures 16C and 16D, we see depicted the effect of percentage of reinforcement composition with spindle speed and depth of cut on SR. In general, lower SR was obtained with lower depth of cut and spindle speed. Here, SR will decrease with the increase of both spindle speed and depth of cut due to variation in reinforcement composition present in the different samples. In addition, a plot of S/N ratios also confirms the irregularity of the results obtained due to the variations in composition of reinforcement.

From Figures 17A–17C, we see depicted the evaluation profile of different percentages of reinforcement composition. The three-dimensional topography of a surface is created by SR, which is a regular or irregular departure from the nominal surface. Traverse feed marks and other irregularities that fall within the parameters of the roughness sampling length are included in this. Roughness is the term used to describe the surface irregularity of longer wavelengths. Based on the profile, an average of the SR value was taken for all the trails, and it is tabulated in Table 4. Due to variation of percentage reinforcement of composition, an influence is exerted over the value of SR, and this is portrayed in Figure 17.

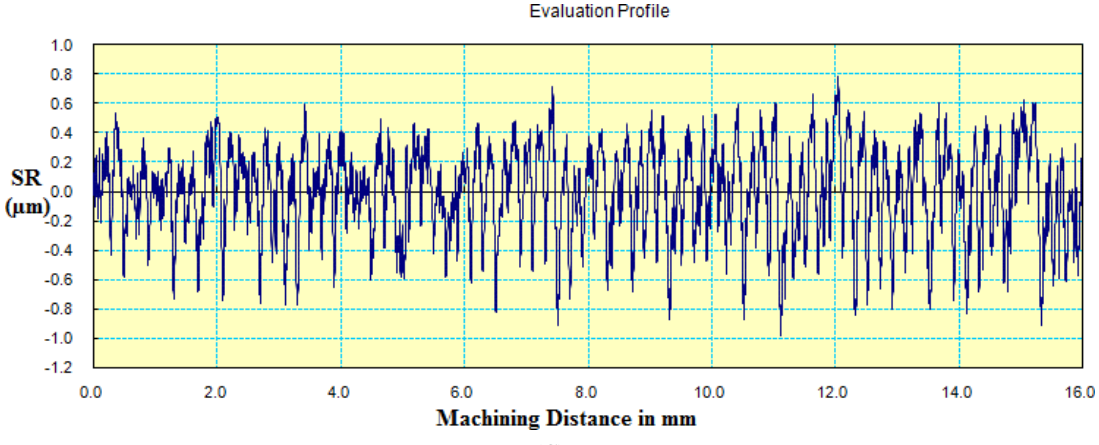
In comparison to a non-reinforced Al alloy, the reinforcement improves the machinability in terms of SR, higher MRR, and a decreased propensity to clog the cutting tool. According to Zhang et al. [21], the addition of SiC particles improved the mechanical properties of the aluminum/SiC composite, which led to SR of the aluminum/SiC composites being lower than that of the aluminum metal during an end-milling experiment.



(A)



(B)



(C)

Fig. 17. Evaluation profile of SR on **(A)** 2.5% of reinforcement composition, **(B)** 5.0% of reinforcement composition, and **(C)** 7.5% of reinforcement composition. SR, surface roughness

4. Conclusions

The Taguchi technique is used in the current study to identify the best parameters for GGBS-reinforced aluminum composites based on L_9 OA. The optimum MRR and SR levels and their control parameters are ascertained using the Taguchi technique.

The following conclusions are drawn from this study:

- The different percentage reinforcement compositions of aluminum composites were fabricated using liquid state stir casting. The addition of GGBS particles in samples of AMC shows clusters of silicon dioxide and oxide particles along the grain boundaries.
- The GGBS particles were found to be uniformly distributed in the aluminum matrix and to properly bond at the interface between the particles and the matrix, according to EDAX observations of the microstructures.
- Various peaks of aluminum composites are seen to rise as the amount of reinforcements increases.
- The Taguchi method was used in this study to choose the best cutting parameters for milling operations on the AMC material out of various combinations of cutting parameters. The feed rate of 260 mm^3/min and the depth of cut of 0.75 mm produced the best MRR value. With respect to MRR, the percentage of composition has an insignificant effect. The best combination for lower SR is a spindle speed of 1,250 rpm, a feed rate of 220 mm^3/min, a depth of cut of 0.25 mm, and 5% reinforcement composition of GGBS.

References

[1] Miracle DB. Metal matrix composites – From science to technological significance. Compos Sci Technol. 2005; 65:2526.

[2] Singh H, Bahri H, Singh KK. Experimental analysis of wear and mechanical characteristics of aluminium matrix composite fabricated through powder metallurgy. In: Computational and experimental methods in mechanical engineering. Singapore: Springer; 2022. pp. 115–29.

[3] Gnanavelbabu A, Surendran KT, Kumar S. Process optimization and studies on mechanical characteristics of AA2014/Al2O3 nanocomposites fabricated through ultrasonication assisted stir–squeeze casting. Int J Met. 2022;16(2):759–82.

[4] Rajan N, Thanigaivelan R, Muthurajan KG. Machinability studies on an A17075 composite with varying amounts of B4C using an induction-heated electrolyte in electrochemical machining. Mater Tehnol. 2019;53(6):873–80.

[5] Dinaharana I, Murugan N, Parameswaran S. Influence of in situ formed ZrB2 particles on microstructure and mechanical properties of AA6061 metal matrix composites. Mater Sci Eng A. 2011;528:5733–40.

[6] Naveen Kumar G, Narayanasamy R, Natarajan S, Kumaresh Babu SP, Sivaprasad K, Sivasankaran S. Dry sliding wear behaviour of AA 6351-ZrB2 in situ composite at room temperature. Mater Des. 2010;31:1526–32.

[7] Michael Rajan HB, Ramabalan S, Dinaharan I, Vijay SJ. Synthesis and characterization of in situ formed titanium diboride particulate reinforced AA7075 aluminum alloy cast composites. Mater Des. 2013;44:438–45.

[8] Zhong L, Zhao Y, Zhang S, Chen G, Chen S, Liu Y. Microstructure and mechanical properties of in situ TiB2/7055 composites synthesized by direct magneto-chemistry melt reaction. Trans Nonferrous Metals Soc China. 2013;23:2502–8.

[9] Zhang S, Zhao Y, Chen G, Cheng X. Microstructures and dry sliding wear properties of in situ (Al3Zr +ZrB2)/Al composites. J Mater Process Technol. 2007;184:201–8.

[10] Zhao Y, Zhang S, Chen G, Cheng X, Dai Q. (ZrB2+Al2O3+Al3Zr)p/Al–4Cu composite synthesized by magneto-chemical melt reaction. Mater Sci Eng A. 2008;487:1–6.

[11] Kumar N, Gautam RK, Mohan S. In-situ development of ZrB2 particles and their effect on microstructure and mechanical properties of AA5052 metal-matrix composites. Mater Des. 2015;80:129–36.

[12] Seeman M, Ganesan G, Karthikeyan R, Velayudham A. Study on tool wear and surface roughness in machining of particulate aluminum metal matrix composite-response surface methodology approach. Int J Adv Manuf Technol. 2010;48(5–8):613–24.

[13] Reddy NSK, Kwang-Sup S, Yang M. Experimental study of surface integrity during end milling of Al/SiC particulate metal–matrix composites. J Mater Process Technol. 2008;201(1–3):574–9.

[14] Kuram E, Ozcelik B. Multi-objective optimization using Taguchi based grey relational analysis for micro-milling of Al7075 material with ball nose end mill. Measurement. 2013;46(6):1849–64.

[15] Thiraviam R, Ravisankar V, Kumar P, Thanigaivelan R, Arunachalam R. A novel approach for the production and characterisation of aluminium–alumina hybrid metal matrix composites. Mater Res Express.

2020;7(4):046512.
[16] Karabulut S, Gökmen U, Çinici H. Optimization of machining conditions for surface quality in milling AA7039-based metal matrix composites. Arab J Sci Eng. 2018;43(3):1071–82.
[17] Manohar G, Maity SR, Pandey KM. Microstructural and mechanical properties of microwave sintered AA7075/Graphite/SiC hybrid composite fabricated by powder metallurgy techniques. Silicon. 2021; 14:5179–89.
[18] Maniraj S, Thanigaivelan R. Optimization of electrochemical micromachining process parameters for machining of AMCs with different % compositions of GGBS using Taguchi and TOPSIS methods. Trans Indian Inst Met. 2019;72(12):3057–66.
[19] Ramesh S, Viswanathan R, Ambika S. Measurement and optimization of surface roughness and tool wear via grey relational analysis, TOPSIS and RSA techniques. Measurement. 2016; 78:63.
[20] Saravanan KG, Sivapragasam A, Prabu R, Maniraj S. Parametric optimization of chrome composite through ultrasonic machining using Taguchi approach. Mate Today Proc. 2021; 45:1975–8.
[21] Zhang GF, Tan YQ, Zhang B. Effect of SiC particles on the machining of aluminum/SiC composite. Mater Sci Forum. 2009; 626:219–24.

Received 2022-10-03
Accepted 2022-12-29